Available online at www.sciencedirect.com
SCIENCE DIRECT
Journal of Solid State Chemistry 179 (2006) 1146–1153
JOURNAL OF SOLID STATE CHEMISTRY
www.elsevier.com/locate/jssc

# Preparation and characterization of microporous $SiO_2$–$ZrO_2$ pillared montmorillonite

Yang-Su Han[a,*], Shoji Yamanaka[b]

[a]*Nanospace Co. Ltd., Business Incubator, Korea Institute of Ceramic Engineering & Technology, 233-5 Gasan-dong Guemcheon-Gu, Seoul 153-801, Republic of Korea*
[b]*Department of Applied Chemistry, Faculty of Engineering, Hiroshima University, Higashi-Hiroshima 739, Japan*

Received 24 August 2005; received in revised form 30 December 2005; accepted 1 January 2006
Available online 3 February 2006

**Abstract**

$SiO_2$–$ZrO_2$ pillared montmorillonite (SZM) was prepared by the reaction of Na-montmorillonite with colloidal silica–zirconia particles which were prepared by depositing zirconium hydroxy cations on silica particles. By pillaring with the colloidal particles, the basal spacing of montmorillonite was expanded to ca. 45 Å and the calcined SZM samples showed large specific surface areas up to 320 $m^2/g$ at 400 °C. In spite of large interlayer separation, adsorption results indicated the presence of micropores generated between the colloidal particles. The microporous structure was maintained at least up to 600 °C and exhibited specific shape selectivity for the adsorption of large organic molecules, especially between toluene and mesitylene. According to the temperature-programmed-desorption (TPD) spectra of ammonia, the calcined SZM showed weakly acidic sites.


*Keywords:* Clays; Pillaring; Microporosity; Nanoparticle; Zirconia

## 1. Introduction

Metal oxide pillared clays derived from the smectites intercalated with inorganic polyoxocations have been attracted extensively as the new type of microporous solid that can serve as shape-selective catalysts, separating agents, supports, sorbents, etc. [1–5]. These materials may have slit-shaped pores whose size are in general larger than conventional zeolites and exhibit specific properties depending on the nature of the pillars. So far various kinds of pillars, including metal polyhydroxycations, metal cluster cations, and colloidal particles, have been intercalated to obtain thermally stable microporous solids [6–25].

Zirconia pillared clays have been attracted considerable attention due to their high thermal stability as acid catalysts for petroleum refining and other acid catalyzed reactions [21–25]. In previous studies [26–32], it was found that clay layers pillared with silica supported metal oxide showed improved thermal stability and high specific surface areas. Since colloidal silica particles are difficult to intercalate between the negatively charged silicate layers, it is necessary to modify the silica surface with metal polycations, which allows the intercalation of colloidal mixed oxide particles into clay.

Recently, it was found that the negatively charged silica particles can be modified with zirconium polyoxocations, which then can easily be introduced between the silicate layers to form $SiO_2$–$ZrO_2$ pillared clays. In the present paper, a systematic route to the $SiO_2$–$ZrO_2$ pillared montmorillonites and their adsorption properties are described.

## 2. Experimental section

### 2.1. Preparation of sol pillared clay

A sodium montmorillonite (Kunipia G supplied by Kunimine Industrial Co.), $Na_{0.35}K_{0.01}Ca_{0.02}(Si_{3.89}Al_{0.11})(Al_{1.60}Mg_{0.32}Fe_{0.08})O_{10}(OH)_2 \cdot nH_2O$ with the cation exchange

*Corresponding author. Fax: +82 2 3282 2455.
*E-mail address:* yshan@inanospace.com (Y.-S. Han).

0022-4596/$ - see front matter © 2006 Elsevier Inc. All rights reserved.
doi:10.1016/j.jssc.2006.01.013

capacity (CEC) of 100 meq./100 g was used. About 1 w/w% aqueous dispersion of the clay was used for the reaction with sol.

A silica sol was prepared as previously reported [26] by mixing silicon tetraethoxide (TEOS, $Si(OC_2H_5)_4$), 2 M HCl and ethanol in a ratio of 41.6 g/10 mL/12 mL at room temperature for 2 h. A 0.2 M-$Zr^{4+}$ aqueous solution was prepared by dissolving the appropriate amount of $ZrOCl_2 \cdot 8H_2O$ in deionized water which was then added dropwisely to the silica sol at a molar ratio of [Si]/[Zr] = 10/1. Then the pH of mixed solution (initial pH = 0.7) was increased to 1.5 by adding a 0.2 M NaOH solution slowly. The dispersion was allowed to stand 1 h at room temperature to facilitate the polymerization of Zr species on the silica surface. This dispersion was mixed with the clay dispersion at a molar ratio Si/Zr/CEC = 50/5/1. The mixture was allowed to stand for 20 h under stirring at room temperature, the products were separated by centrifugation, washed with ethanol/water (1:1 volume ratio) several times to remove the excess silica sol, and then dried in a stream of dry air at room temperature. The dried samples were calcined for 2 h at 200–800 °C in air.

### 2.2. Characterization of pillared clay

Before air-drying, a small portion of the wet product was spread on a quartz glass slide for X-ray powder diffraction (XRD) (SRA-M18XHF, MAC Science Co., graphite monochromator, Cu$K\alpha$). Thermogravimetric analysis (TG) analysis was performed on the dried samples with a heating rate of 5 °C/min and under the stream of oxygen–nitrogen mixture (flow rate $N_2$:$O_2$ = 100:100 mL/min.). Infrared spectra (IR) of KBr disks were recorded with a Perkin-Elmer FT-IR spectrometer. Elemental analysis of the pillared products was carried out by ICP (Perkin Elemer OPTIMA 3000) on a sample melted with lithium metaborate at 900 °C and dissolved in a 3% $HNO_3$ solution.

Adsorption–desorption isotherms for nitrogen were measured volumetrically at 77 K by a computer-controlled measurement system. All samples were degassed at 200 °C for 2 h under reduced atmosphere prior to the adsorption measurement. Adsorption–desorption isotherms for some selected solvent vapors having different molecular sizes were also measured gravimetrically at 25 °C by using a CAHN balance.

Temperature-programmed-desorption (TPD) spectra of ammonia were recorded by gas chromatography with a thermal conductivity detector. About 200 mg of the sample were reheated in a stream of helium for 1 h at 400 °C and cooled down to room temperature. Then the sample was exposed to 1 atm of ammonia for 30 min, and the excess ammonia was purged out in a flow of helium at room temperature for 5 h. The measurement was carried out up to 550 °C at a heating rate of 5 °C/min and a helium flow rate of 100 mL/min.

## 3. Results and discussion

### 3.1. Preparation of colloidal $SiO_2$–$ZrO_2$ particles

In the preparation of oxide pillared clay, the most important step is to obtain positively charged colloidal particles with moderate stability in aqueous solutions. As previously reported [33], hydrolysis of TEOS yields spherical silica particles. Since the resulting particles are negatively charged, it is necessary to recharge the particles to intercalate them into montmorillonite.

Dissolution of Zr(IV) salts in water is known to result initially in a tetrameric cation species, $Zr_4(OH)_8^{8+}$ [34,35]. During aging highly polymerized Zr-species become dominant, and further polymerization eventually results in the precipitation of hydrated $Zr(OH)_4$. Increased pH, high temperature, and extended aging periods increase the degree of polymerization and, subsequently, rise the surface areas and basal spacings of the pillared clays. In the presence of silica sol, however, such conditions for enhancing the polymerization are not applicable due to the formation of unavoidable mixed gels. In the present study, it was found that pH = 1.5 was suitable to obtain stable

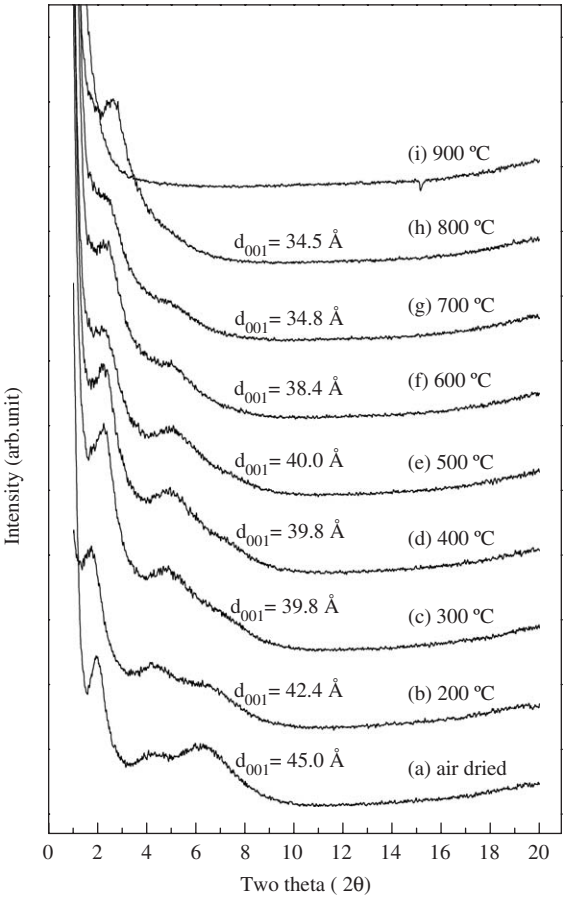


Fig. 1. X-ray diffraction patterns of the $SiO_2$–$ZrO_2$ pillared montmorillonites: (a) air-dried and heated for 2 h (b–i).

$Zr_x(OH)_y$–$SiO_2$ sol. Even though the pH condition is not sufficient for obtaining highly polymerized Zr species, the negatively charged silica surface becomes positive by depositing of Zr cationic species. Since the tetrameric $Zr_4(OH)_8^{8+}$ species is expected to be formed exclusively without disturbing by other Zr species at the pH of 1.5 [34,35], the size of Zr modified silica particles would be quite uniform.

### 3.2. X-ray diffraction

By pillaring with colloidal $SiO_2$–$ZrO_2$ particles, the basal spacing of the clay layer is increased from 9.6 Å to ca. 45 Å, and higher order reflections (at least 2nd) are observed, suggesting the colloidal particles are intercalated in an ordered manner (Fig. 1). Though the basal spacing gradually decreases on heating due to the contraction of the pillars and dehydroxylation of silicate, a distinct (001) reflection can be seen at least up to 800 °C, reflecting the regularity of the two-dimensional layer structure is fairly well retained at this temperature.

Table 1
Chemical analysis of $SiO_2$–$ZrO_2$ pillared clay

| Analytical results (mol%) | | | Pillar compositions[a] | | |
|---|---|---|---|---|---|
| $SiO_2$ | $ZrO_2$ | $Al_2O_3$ | $SiO_2$ ($x$) | $ZrO_2$ ($y$) | $x+y$ |
| 77.4 | 6.5 | 13.1 | 6.24 | 0.84 | 7.08 |

[a]The compositions ($x$ and $y$) are given as $(SiO_2)_x$ and $(ZrO_2)_y$ per formula with $[(Si_{3.89}Al_{0.11})\ (Al_{1.60}Mg_{0.32}Fe_{0.08})]O_{10}(OH)_2$.

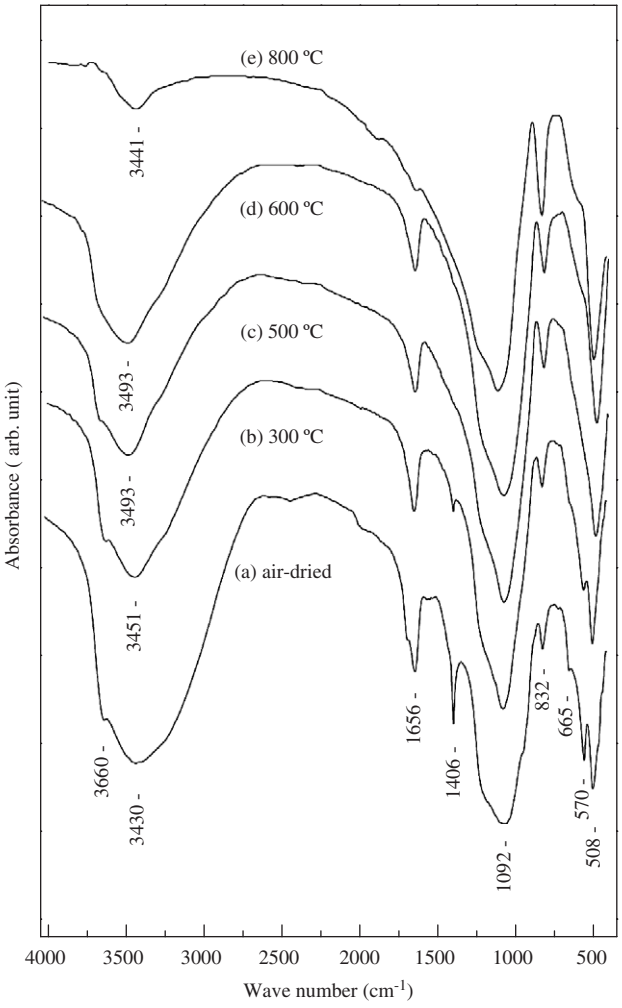


Fig. 3. FT-IR spectra of the $SiO_2$–$ZrO_2$ pillared montmorillonites: (a) air-dried and heated at (b) 300 °C, (c) 500 °C, (d) 600 °C, and (e) 800 °C for 2 h.

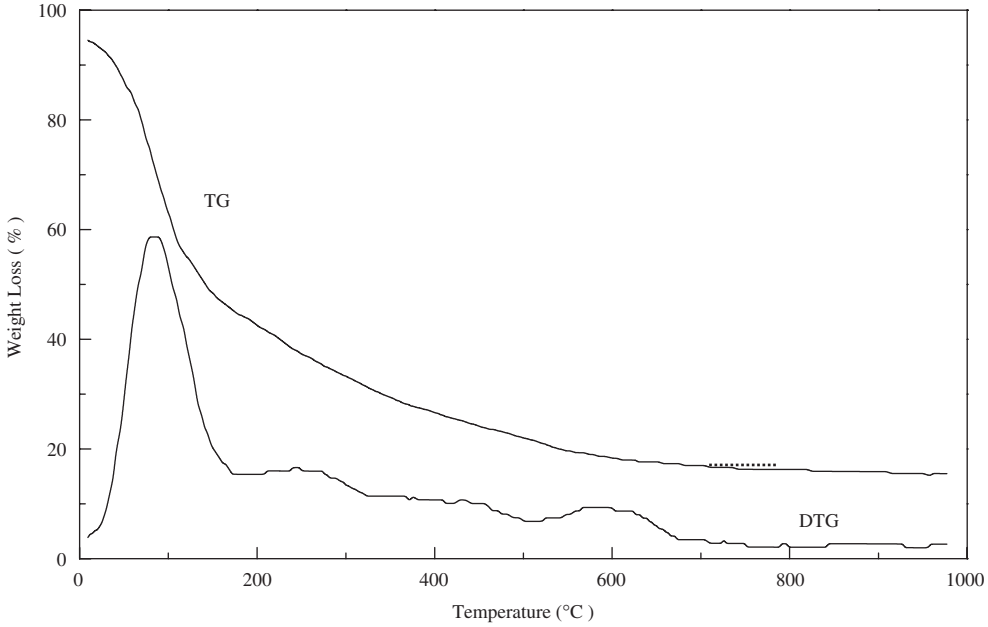


Fig. 2. TG-DTG curves of air-dried $SiO_2$–$ZrO_2$ pillared montmorillonite.

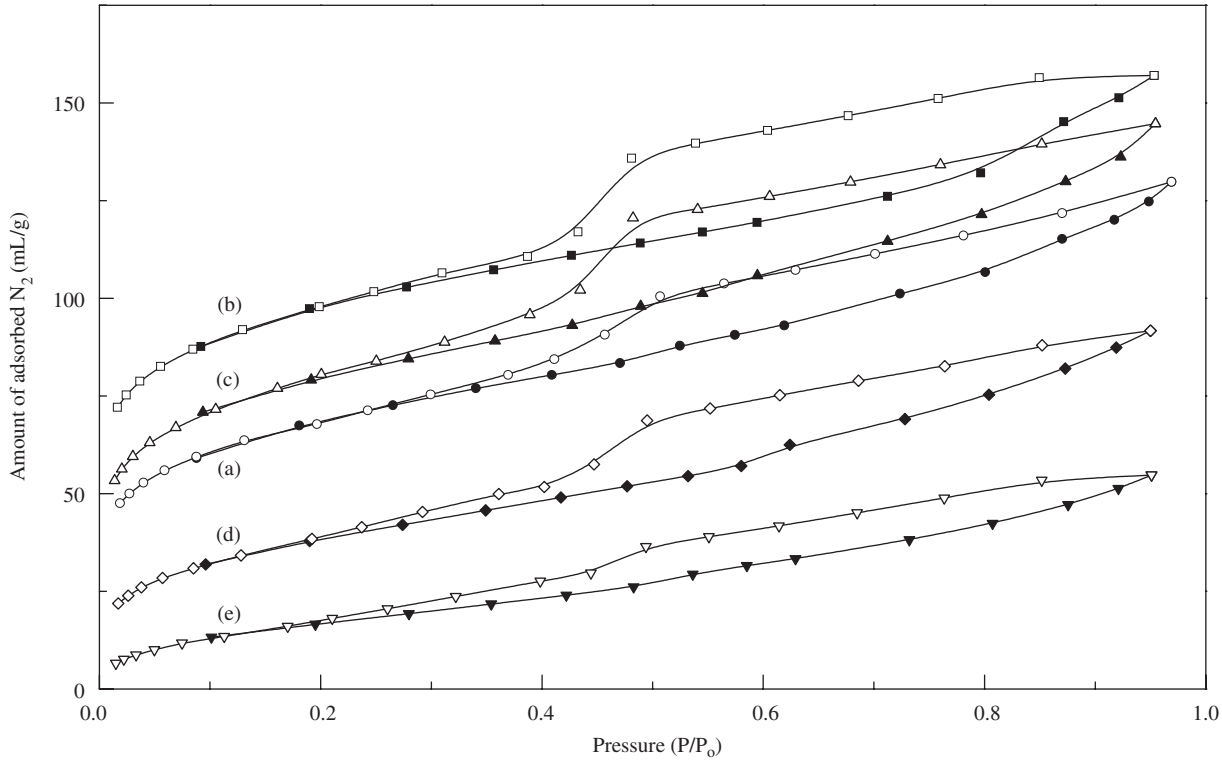


Fig. 4. Nitrogen adsorption–desorption isotherms at 77 K for the $SiO_2$–$ZrO_2$ pillared montmorillonites heated at (a) 300 °C, (b) 400 °C, (c) 500 °C, (d) 600 °C, and (e) 700 °C for 2 h.

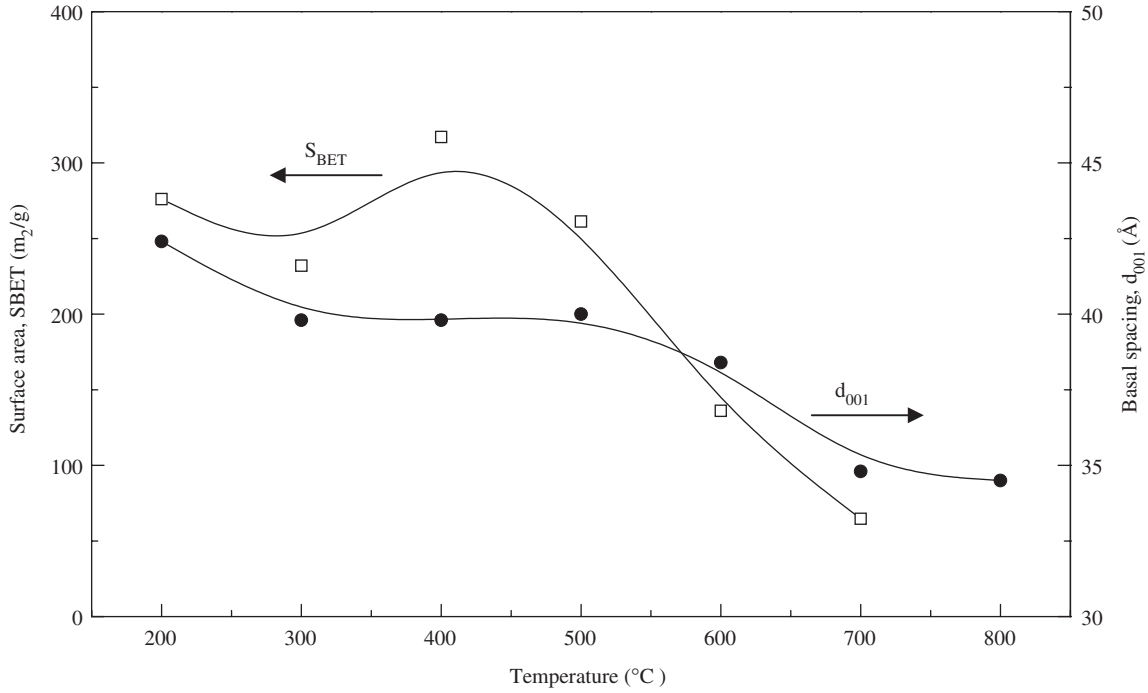


Fig. 5. Basal spacing ($d_{001}$) and surface area ($S_{BET}$) as a function of heating temperature.

### 3.3. Elemental analysis

Using the structural composition of the starting Na-montmorillonite and assuming that the tetrahedral and octahedral occupancy by Si and Al is unchanged, the structural formula of the pillared product is estimated (Table 1). The amount of $SiO_2$ coming from the silicate layer is evaluated from the $Al_2O_3$ content and subtracted from the total $SiO_2$. In the formula basis, 7 mol oxides are taken up by the clay.

### 3.4. Thermogravimetric analysis

The first drastic weight loss below 200 °C can be attributed to the loss of physisorbed or loosely coordinated water (Fig. 2). Subsequent weight loss in the temperature range of 200–500 °C might be related to the dehydration of interlayer pillars. An additional loss at around 550 °C can be assigned to the dehydroxylation of silicate layers of the clay. From this analysis, it is expected that a stable microporous structure can be obtained after calcinig at range of 300–500 °C.

### 3.5. Infrared spectroscopy

IR spectroscopy provides complementary evidence for the structural change during the thermal treatment of pillared products. In the air-dried sample (Fig. 3a), most absorption bands are typical for smectites [36]. An additional strong and sharp absorption band at $\sim$1400 $cm^{-1}$ might be due to the vibration of OH groups of the intercalated zirconium species which decreases drastically after heating at 300 °C (Fig. 3b). On heating to 500 °C (c), the absorption band at 3660 $cm^{-1}$ corresponding to the stretching vibrational mode of structural OH groups of the silicate is significantly reduced, and disappears almost completely after calcining at 600 °C (d), indicating the dehydroxylation of octahedral layers in silicates have finished below this temperature which is consistent with the result of thermal analysis.

### 3.6. Nitrogen adsorption–desorption isotherm

The nitrogen adsorption isotherms are plotted in Fig. 4. These can be classified as Type I according to the BDDT classification [37], indicating that most of the nitrogen is adsorbed in micropores. The adsorption isotherms for the samples calcined below 500 °C are fitted by the Langmuir equation, while the isotherms of samples heated to higher temperatures are well fitted by the BET equation. The micropores formed at lower temperature (< 500 °C) disappear gradually with increasing temperature due to the sintering of the intercalated particles and, as a consequence, the contribution of mesopores becomes more significant. Most of the micropores are destroyed after calcining at 700 °C (e). Sintering seems to take place during the dehydroxylation of silicate layers at around 600 °C.

The surface area reaches a maximum ($\sim$320 $m^2/g$) at 400 °C, then decreases linearly with temperature (Fig. 5 and Table 2). The increase of the surface area at lower temperature is due to the condensation of interlayer pillars to oxides, which creates micropores between the intercalated particles.

The micropore size distribution curves of the calcined SZM samples are calculated by the method of Mikahail

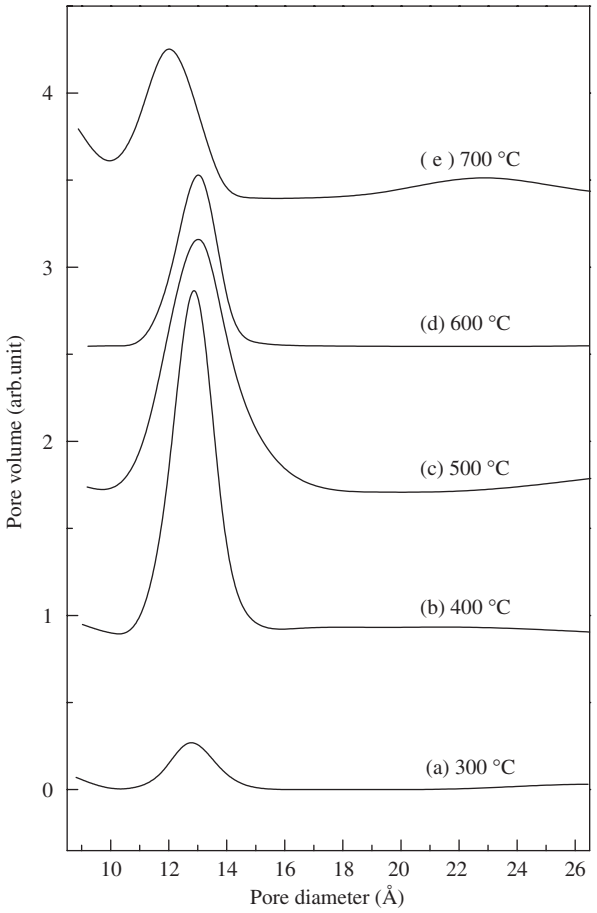


Fig. 6. Micropore pore size distribution of the $SiO_2$–$ZrO_2$ pillared montmorillonites heated at (a) 300 °C, (b) 400 °C, (c) 500 °C, (d) 600 °C, and (e) 700 °C for 2 h.

Table 2
Basal spacings and pore structure parameters of $SiO_2$–$ZrO_2$ pillared clays

| Calcination temp. (°C) | Basal spacing (Å) | Surface area ($m^2/g$) | | | Pore volume (mL/g) | |
|---|---|---|---|---|---|---|
| | | BET | Lang. | $S_{micro-}$[a] | Total | $V_{micro-}$[a] |
| 200 | 42.4 | 232 | 356 | 90 | 0.20 | 0.05 |
| 300 | 39.8 | 276 | 398 | 188 | 0.20 | 0.10 |
| 400 | 39.8 | 317 | 489 | 203 | 0.24 | 0.11 |
| 500 | 40.0 | 261 | 407 | 98 | 0.22 | 0.06 |
| 600 | 38.4 | 136 | 220 | — | 0.14 | — |
| 700 | 34.8 | 65 | 112 | — | 0.08 | — |

[a]Estimated by *t*-plot method.

et al. (MP method) [38] using the adsorption branches of the isotherms. As illustrated in Fig. 6, the pore size of the pillared clays shows a micropore region of 12–14 Å. The portion of micropore volume is reached to maximum after calcining at 400 °C (b), then the portion is gradually decreased as the calcining temperature is increased. At 700 °C (e), the peak maximum shifts to smaller pore sizes along with the drastic reduction in the portion of micropore volume. The decrease in micropore volume is mainly due to the pore narrowing by sintering of small micropores.

### 3.7. Solvent adsorption–desorption isotherm

Adsorption–desorption isotherms for some selected solvents with different molecular sizes were measured at 25 °C on the sample calcined at 400 °C (Fig. 7). The adsorption isotherms for larger molecules such as toluene and mesitylene fit the Langmuir plot, whereas that of water molecule fits the BET plot. The adsorption isotherm for methanol fits the Langmuir as well as the BET equation, indicating that the multilayer adsorption of methanol molecules is restricted due to the limited pore size.

Comparison to toluene, the adsorption of mesitylene is strongly reduced. SZM has high shape-selectivity to toluene against mesitylene due to its limited pore size. This finding also suggests that the pore size is approximately in the order of the molecular size of toluene (~6 Å). This is well consistent with the result that the nitrogen adsorption isotherm fits well the Langmuir equation for a monolayer adsorption.

### 3.8. Structural model

By pillaring the Zr-modified silica particles, the basal spacings are expanded as large as 45 Å. Moreover, the interlayer arrangement of the particles seems to be uniform as revealed by higher order X-ray reflections (Fig. 1). But, the nitrogen (Fig. 4) and solvent adsorption (Fig. 7) results strongly suggest that the pores are much smaller than the basal spacing. As previously suggested for $SiO_2$–$TiO_2$ sol pillared clays [26,27], the double-layer arrangement of sol particles would be expected where micropores are formed in the interstices between sol particles and silicate layers of clay as schematically shown in Fig. 8.

Even though, a distinct diffraction peak (00l) due to layer structure can be seen up to 800 °C (Fig. 1), the micropores are almost disappeared after heating above 600 °C. This can be explained as follows. Although the decomposition of the structural OH groups of

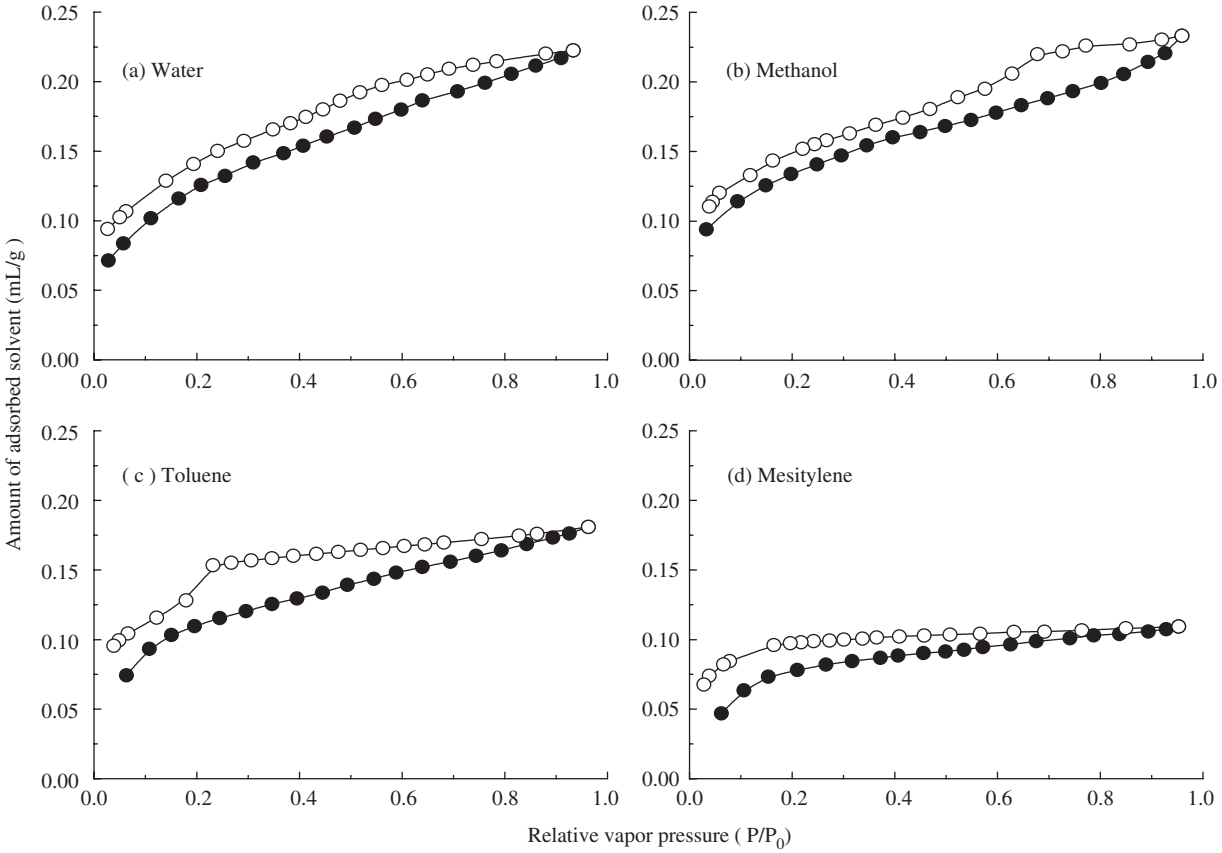


Fig. 7. Solvent adsorption–desorption isotherms for the $SiO_2$–$ZrO_2$ pillared montmorillonites heated at 400 °C: (a) water, (b) methanol, (c) toluene, and (d) mesitylene.

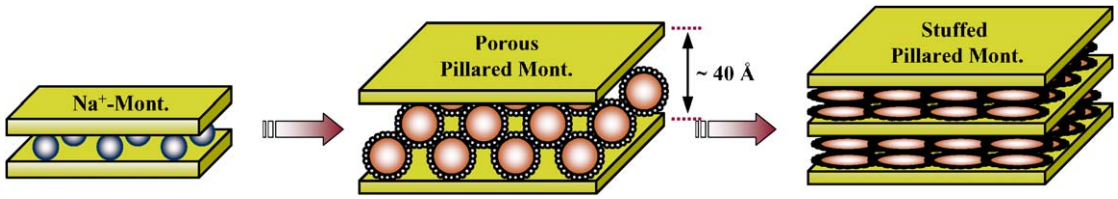


Fig. 8. Schematic structural model of $SiO_2$–$ZrO_2$ pillared montmorillonite.

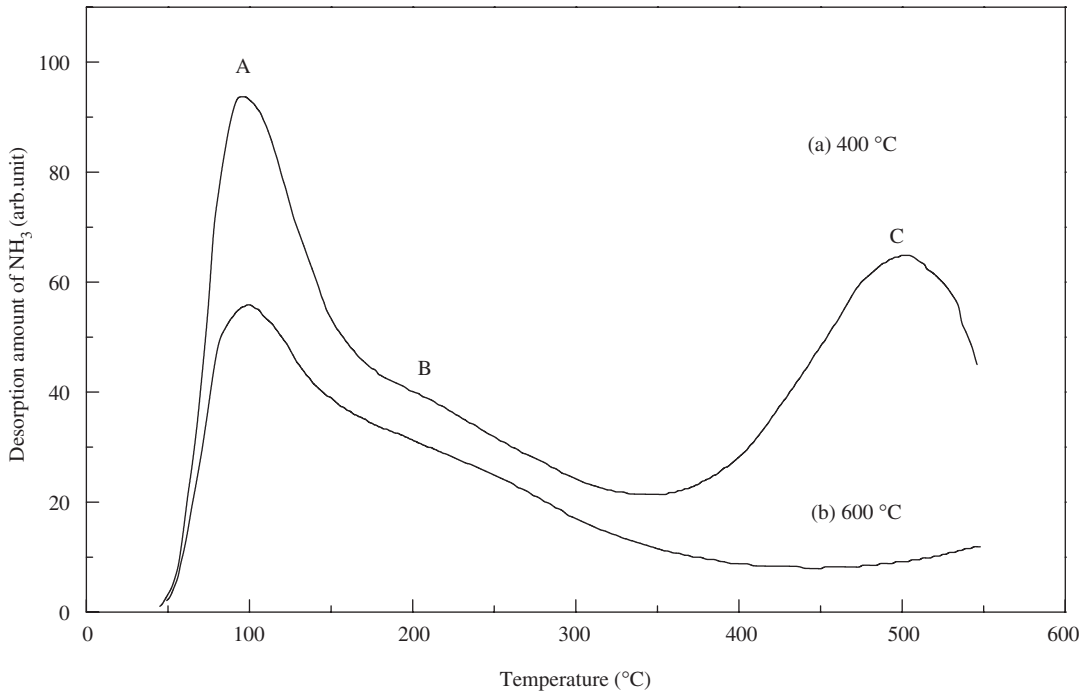


Fig. 9. Temperature-programmed-desorption (TPD) spectra of ammonia for the $SiO_2$–$ZrO_2$ pillared montmorillonites heated at (a) 400 °C and (b) 600 °C for 2 h.

di-octahedral smectites occurs near 600 °C (Fig. 2 and Fig. 3), the framework of the silicate layer can be stabilized up to higher temperatures if the OH groups are converted to $O^{2-}$ ions by the condensation with oxides or hydroxides in between the silicate layers. The sintering of pillars also begins beyond 600 °C, resulting in a partial pore-narrowing or blocking which makes the nitrogen molecules inaccessible to pores due to the steric hindrance. But the sintered sol particles may remain in an ordered manner to some extent up to higher temperature, giving rise to the 'stuffed' pillared structure (Fig. 8).

### 3.9. Acidic property

To investigate the acidic nature of $SiO_2$–$ZrO_2$ pillared montmorillonite, the TPD spectra of ammonia were measured on SZM samples heated to 400 °C (Fig. 9a) and 600 °C (Fig. 9b). The strong desorption peaks at around 100 °C (peak A) are assigned to the dissociation of ammonia weakly bound on weak acidic centers or physically adsorbed on the surface or in the pores.

The second dissociation peaks at about 200–300 °C (peak B) are very weak in intensity, but are observed clearly even after calcining at 600 °C (Fig. 9b). Since the Brönsted acidic sites usually disappear after heating above 400 °C, the second peaks might originate from Lewis acid sites developed during the thermal treatment. Because most of pillar surfaces are covered by $ZrO_2$ and due to the electroneutrality of the Zr–O–Si linkage, however, the population of such sites would be low and the acidic strength is weak, resulting in low intensity and low ammonia desorption temperature in the TPD spectra.

In the sample calcined at 400 °C (Fig. 9a), another strong desorption peak is seen at above 400 °C (peak C), which disappears after calcining at 600 °C (Fig. 9b). Even though further study is needed, the peak C might be composed of the desorption of ammonia bound tightly to strong Brönsted acid sites which are generated by hydrolysis of the polynuclear hydroxy species during heating and the desorption of water produced by dehydroxylation of the silicate layers.

## 4. Conclusions

Montmorillonite pillared with colloidal particles was prepared by ion-exchange of the Na-montmorillonite with $SiO_2$–$ZrO_2$ particles obtained by titrating a $Zr^{4+}$ aqueous solution with NaOH in the presence of silica particles. The basal spacing was expanded as large as 45 Å. In spite of such a large interlayer separation, adsorption data strongly suggested the presence of micropores, leading to a multi-layer stacking model of interlayered colloidal particles where micropores are formed in the interstices between the colloidal particles. Due to the limited pore size, the SZM exhibited a shape-selectivity to the adsorption of mesitylene molecules. The calcined SZM samples showed high specific surface areas up to $320\,m^2/g$, and the microporous structure was retained at least up to 600 °C. According to the TPD spectra of ammonia, the $SiO_2$–$ZrO_2$ pillared montmorillonite heated at 600 °C seemed to possess weak Lewis acid sites.

## Acknowledgment

This work was financially supported by the SMBA of Korea through the Technology Innovation R & D Program (2005).

## References

[1] R. Burch (Ed.), Pillared clays, Catal. Today 2 (1988).
[2] E.M. Serwicka, K. Bahranowski, Catal. Today 90 (2004) 85.
[3] A. Sayari, M. Jaroniec, T.J. Pinnavaia (Eds.), Nanoporous Materials II, Elsevier, Tokyo, 2000.
[4] K. Ohtsuka, Chem. Mater. 9 (1997) 2039.
[5] J.T. Kloproge, J. Porous Mater. 5 (1998) 5.
[6] G.W. Brindley, R.E. Sempels, Clay Miner. 12 (1977) 229.
[7] S. Yamanaka, G.W. Brindley, Clays Clay Miner. 26 (1978) 21.
[8] T.J. Pinnavaia, M.S. Tzou, S.D. Landau, J. Am. Chem. Soc. 107 (1985) 4783.
[9] N. Maes, I. Heylen, P. Cool, E.F. Vansant, Appl. Clay Sci. 12 (1997) 43.
[10] M. Sychev, V.H.J. de Beer, R.A. van Santen, Microporous Mater. 8 (1997) 255.
[11] M.J. Hernando, C. Pesquera, C. Blanco, I. Benito, F. González, Chem. Mater. 8 (1996) 76.
[12] K.B. Brandt, R.A. Kydd, Chem. Mater. 9 (1997) 567.
[13] X. Tang, W.-Q. Xu, Y.-F. Shen, S.L. Suib, Chem. Mater. 7 (1995) 102.
[14] S. Moreno, R. Sun Kou, G. Poncelet, J. Phys. Chem. B 101 (1997) 1569.
[15] K. Mogyorosi, I. Dékány, J.H. Fendler, Langmuir 19 (2003) 2938.
[16] C. Ooka, H. Yoshida, K. Suzuki, T. Hattor, Micro. Meso. Mater. 67 (2004) 143.
[17] S. Yamanaka, T. Nishihara, M. Hattori, Y. Suzuki, Mater. Chem. Phys. 17 (1987) 87.
[18] J. Ahenach, P. Cool, R.E.N. Impes, E.F. Vansant, J. Porous Mater. 35 (1986) 377.
[19] F. Kooli, J. Bovey, W. Jones, J. Mater. Chem. 7 (1997) 153.
[20] G. Fetter, D. Tichit, P. Massiani, R. Dutartre, F. Figueras, Clays Clay Miner. 42 (1994) 161.
[21] S. Yamanaka, G.W. Brindley, Clays Clay Miner. 27 (1979) 119.
[22] G.J.J. Bartley, Pillared clays, in: R. Burch (Ed.), Catalysis Today, Elsevier, Amsterdam, 1988, p. 233.
[23] F. Kooli, W. Jones, J. Mater. Chem. 8 (1998) 2119.
[24] R. Toranzo, M.A. Vicente, M.A. Banares-Munoz, L.M. Gadia, A. Gil, Micro. Meso. Mater. 173 (1998) 173.
[25] K. Ohtsuka, Y. Hayashi, M. Suda, Chem. Mater. 5 (1993) 1823.
[26] S. Yamanaka, Y. Inoue, M. Hattori, F. Okumura, M. Yoshikawa, Bull. Chem. Soc. Jpn. 65 (1992) 2494.
[27] S. Yamanaka, Am. Ceram. Soc. Bull. 70 (1992) 1056.
[28] Y.-S. Han, H. Matsmoto, S. Yamanaka, Chem. Mater. 9 (1997) 2013.
[29] Y.-S. Han, S. Yamanaka, J. Porous Mater. 5 (1998) 111.
[30] Y.-S. Han, J.H. Choy, J. Mater. Chem. 8 (1998) 1459.
[31] Y.-S. Han, S. Yamanaka, J.H. Choy, Appl. Catal. A 174 (1998) 83.
[32] Y.-S. Han, S. Yamanaka, J.H. Choy, J. Solid State Chem. 144 (1999) 45.
[33] S. Sakka, K. Kamiya, K. Makita, Y. Yamamoto, J. Non-Cryst. Solids 63 (1984) 223.
[34] A. Clearfield, Inorg. Chem. 3 (1964) 146.
[35] A. Clearfield, J. Mater. Res. 5 (1990) 161.
[36] D.T.B. Tennakoon, J.M. Thomas, W. Jones, T.A. Carpenter, S. Ramdas, J. Chem. Soc. Faraday Trans. 82 (1986) 545.
[37] S.J. Gregg, K.S.W. Sing (Eds.), Adsorption, Surface Area and Porosity, Academic Press, London, 1982.
[38] R.S. Mikahail, S. Brunauer, E.E. Bodor, J. Collid. Inter. Sci. 26 (1968) 54.